Computer Modeling in Engineering & Sciences CMES, vol.122, no.1, pp.175-205, 2020

Observability Analysis in Parameters Estimation of an Uncooperative Space Target

Xianghao Hou[1,*] and Gang Qiao[1]

Abstract: To study the parameter estimating effects of a free-floating tumbling space target, the extended Kalman filter (EKF) scheme is utilized with different high-nonlinear translational and rotational coupled kinematic & dynamic models on the LIDAR measurements. Applying the aforementioned models and measurements results in the situation where one single state can be estimated differently with varying accuracies since the EKFs based on different models have different observabilities. In the proposed EKFs, the traditional quaternions based kinematics and dynamics and the dual vector quaternions (DVQ) based kinematics and dynamics are used for the modeling of the relative motions between a chaser satellite and an uncooperative target. In the non-contact estimating scenarios, only highly nonlinear relative attitude and range measurements: the grapple fixture on the target measured from the chaser satellite via vision-based sensors, can be used. By evaluating the results of the EKFs, the observability properties of each EKF are studied analytically and numerically with the the Observability Gramian matrices (OG) and the standard deviations for every estimated parameters. The analysis of observability perform intensive studies and reveal the intrinsic factors that affect the accuracy and stability of the parameters estimation of an uncooperative space target. Finally, the analytical and numerical results show the optimal composition of the kinematic & dynamic models and measurements.

Keywords: Parameter estimations, observability analysis, dual quaternions, extended Kalman filter.

1 Introduction

In recent years, the on-orbit service missions aiming at uncooperative space targets have attracted a number researchers [Flores-Abad, Ou, Pham et al. (2014); Jankovic, Paul and Kirchner (2015); Ma, Dai and Yuan (2017); Dai, Jing, Yu et al. (2018)]. Since the uncooperative space targets are usually malfunctioning and tumbling in space, good parameter estimations are critical for the future tracking and capturing procedures. To

[1]Acoustic Science and Technology Laboratory and College of Underwater Acoustic Engineering, Harbin Engineering University, Harbin, 150001, China.

[*]Corresponding Author: Xianghao Hou. Email: houxianghao1990@163.com.

Received: 26 August 2019; Accepted: 16 September 2019.

achieve reasonable results in parameter estimations of a free-floating tumbling space target, different kinematic & dynamic models, different types of measurements accompanied by various kinds of estimating algorithms have been utilized by a number of researchers [Hou, Ma, Wang et al. (2017); Razgus, Mooij and Choukroun (2017); Aghili (2012); Segal and Gurfil (2012); Filipe, Kontitsis and Tsiotras (2015)]. Although the research on parameter estimations of the uncooperative space targets are extensive, the intrinsic factors that affect the accuracies and stabilities of them are given a lesser attention.

Xing et al. [Xing, Cao, Zhang et al. (2010); Segal and Gurfil (2012)] considered the relative orbital motions and set up an orbital relative kinematic model under the effects of the translational and rotational coupled effects to have the relative pose parameters estimated. Also, Aghili et al. [Aghili (2012); Aghili and Parsa (2009)] showed an approach by modeling the translational motions and rotational motions separately; however, in case of the uncooperative space target, the translational and rotational coupled effect must be considered, since the grapple fixture of the target is usually away from its centre of mass. Razgus et al. [Razgus, Mooij and Choukroun (2017); Filipe and Tsiotras (2013b,a); Filipe, Kontitsis and Tsiotras (2015)] utilized dual quaternions based relative kinematic equations to depict the relative motion between an uncooperative space target and a chaser satellite. In addition, by applying this model, it can be shown that the relative pose parameters are well estimated. By using the error quaternions to represent the relative attitude motions, Hou et al. [Hou, Ma, Wang et al. (2017)] proposed a dual vector quaternions (DVQ) based method to model the relative kinematics and dynamics of an uncooperative space target. With this modeling technique, not only the pose parameter but also the inertial parameters are estimated at the same time. For an uncooperative and tumbling target in space, only the contactless measurements are available. Under this circumstance, the vision-based sensors are the most widely used measurement technique. Liu et al. [Liu and Hu (2014)] utilized a monocular camera to obtain the relative attitude between the chaser satellite and the uncooperative space target. Dong et al. [Dong and Zhu (2015)] utilized a stereo vision camera to measure both the relative attitude and range. Nevertheless, the accuracies of the passive imagers are strongly affected by the space environment [Opromolla, Fasano, Rufino et al. (2017)] and the active imager-LIDAR system is widely used in the measurements of a free-floating tumbling space target [Aghili (2012); Aghili and Parsa (2009)]. As proposed by Kalman [Kalman (1960)], Kalman filter (KF) has become the de facto estimating technique due to its efficient and reliable estimations. By applying the first order Taylor series expansion to linearize the nonlinear system equations [Lefferts, Markley and Shuster (1982)], the extended Kalman filter (EKF) has been successfully used in various parameters estimating missions. Aghili et al. [Aghili (2012); Aghili and Parsa (2009)] utilized the EKF to estimate the attitude quaternions and inertial parameters of a free-floating tumbling space target. Additionally, Hou et al. [Hou, Ma, Wang et al. (2017)] designed a DVQ based EKF to have the similar parameters estimated. Moreover, Lefferts et al. [Lefferts, Markley and Shuster (1982)] designed an EKF based estimating algorithm and estimated the parameters of a cooperative spacecraft. In recent years, new approaches have been proposed: unscented

Kalman Filters (UKF) [Crassidis and Markley (2003)] and particle filters (PF) [Yang and Crassidis (2004)] aiming to enhance the estimating ability, both with a set of drawbacks [Crassidis, Markley and Yang (2007)]. As mentioned by Crassidis et al. [Crassidis, Markley and Yang (2007)] EKF is still the workhorse of the estimating techniques due to its robustness and reliable parameters estimating scheme. Furthermore, by calculating the Jacobian matrix of the system, some intrinsic attributes (i.e., the derivatives of each parameter with the other state, the relationship between one parameter and the other ones, etc.) can be revealed.

When working on the effects of the parameters estimating problems, the observability analysis of the designed estimating algorithm is vital. The observability is a tool showing whether the parameters of a system can be estimated from the measurements accurately. If a system is fully observable, all the parameters of it can be determined from the measurements within finite time. If a system is not fully observable but with high observability, the parameters of the system will have better estimations or easier to be estimated than the ones in a system with lower observability. However, the accuracies of the estimations of parameters in a not fully observable system can not be guaranteed [Ablin (1967); Ham and Brown (1983); Wilson and Guhe (2005); Krener and Ide (2009)].

As a consequence, the analysis of observability is quite important for one to design a parameter estimating algorithm. The first goal is to make the selected system and measurement that consist of one algorithm have full observability. If this goal cannot be achieved, an algorithm with the combination of system model and measurements of higher observability should be considered. A higher observability stands for the robustness of the estimating results to the noise and easier to be determined from the measurements [Yu, Cui and Zhu (2014); Friedman and Frueh (2018); Zanetti and DSouza (2015)]. By applying different kinematic and dynamic models on different types of measurements, the final estimating results will be of a various accuracy. Good observability shows the parameter estimations have high accuracies and the parameter estimating process is more stable. In the analysis of the observability of a certain system, the Lie algebra is often utilized [Liu (2006)].

Huxel [Huxel (2009)] utilized a Lie algebra based method to analyze the observability of various kinds of space missions. However, the research can only determine whether the system is observable or not, and hence not the level of observability. Yu et al. [Yu, Cui and Zhu (2014)] proposed an alternative for calculation of the observability matrix and provided a level of observability of the system by analyzing the observability matrix. In addition, Butcher et al. [Butcher, Wang and Lovell (2017)] utilized the Lie algebra based method along with the analysis of the observability matrix to show the system observability. However, the observability matrix calculated by Lie algebra needs to compute the high order Lie derivatives which will cost a lot of computational resources when the states to be estimated have high dimensions. Also, the observability matrix calculated by Lie derivatives cannot have the information of the noise of the measurements [Butcher, Wang and Lovell (2017)].

However, the covariance of the measurement noise will affect the observability analyzing results since the noise can make change on the measurements [Friedman and Frueh (2018)]. If a system is observable or has good observability, the changes made by the measurement will have little affect on the estimating results. On the contrary, if the observability of a system is low, the small change made by noise will affect the results seriously [Krener and Ide (2009)]. By calculating the Jacobi matrix and linearizing the nonlinear system, the Observability Gramian (OG) can be computed. Although the error of the linearization will exist during this procedure, the effects to the analysis of the observability of the system are quite limited [Zanetti and DSouza (2015)]. Considering the effects of the measurement noise, Chaves-Jimenez et al. [Chaves-Jiménez, Guo and Gill (2017)] utilized the OG method to analyze the observability for a spacecraft in the low earth orbit. By utilizing the OG method, the observability matrix can be calculated in each time step without computing the high order Lie derivatives, which is suitable for high dimensional systems.

To the best of the authors' knowledge, no research on the analysis of the effects of parameter estimations for a free-floating tumbling space target has been published at the time of writing. Without deeper research on the subject, the intrinsic factors affecting the accuracy and stability of the estimating methods cannot be derived. This paper focuses on two kinds of kinematic & dynamic models as well different LIDAR measurements (i.e., relative attitude measurements and range measurements): 1) traditional quaternions based kinematics and dynamics model; 2) DVQ based kinematics and dynamics model (considering the translational and rotational coupled effects). With these system models, EKFs with different models are proposed. In addition, the observability matrix is calculated and analyzed analytically and numerically by its rank and Condition number. Moreover, by calculating the eigenvalues and eigenvectors of the observability matrix, the level of the observability of each state is revealed [Ablin (1967); Ham and Brown (1983)]. Furthermore, the time evolution of the covariance matrix of each system model is calculated to test the system observability. By utilizing the analysis contained in this paper, the intrinsic factors that affect the results of the parameter estimations of a free-floating tumbling space target are revealed. Also, by applying methods described in this paper, the optimal composition of the kinematic & dynamic models and measurements can be selected to increase the accuracy and stability of the results. This paper is organized as follows. Section 2 gives a review of the DVQ based kinematics and dynamics along with the traditional kinematics and dynamics. Then, the models of LIDAR measurements are described in Section 3. Also, based on the aforementioned models, different EKF based estimating algorithms are designed. Section 4 described method for calculation of the observability matrix for each EKF based estimating algorithm by using the OG method. Also, the rank and condition number of the observability matrix are calculated. Moreover, the covariance time evolution analysis are made in Section 4. Followed by the mathematical simulations and relative discussions in Section 5. Finally, the conclusions are drawn in Section 6.

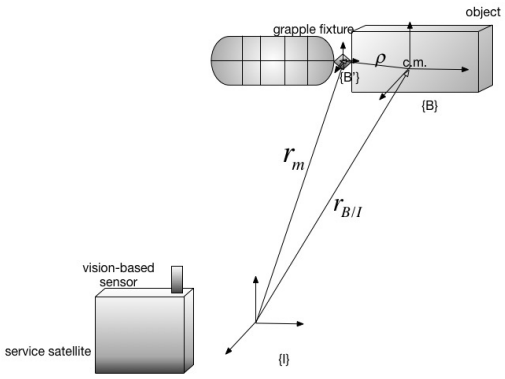

Figure 1: Model of the chaser satellite and the uncooperative space target [Hou, Ma, Wang et al. (2017)]

2 Model kinematics and dynamics

Firstly, the overview of the parameter estimations scenario is shown in Section 2.1. Then four kinds of model kinematics and dynamics are given in Section 2.2 to Section 2.5, namely: 1) Model kinematics based on traditional quaternions; 2) Traditional model kinematics and dynamics; 3) DVQ based model kinematics; 4) DVQ based model kinematics and dynamics. The definitions and basic calculation lemmas for quaternions and dual quaternions can be found in literature [Hou, Ma, Wang et al. (2017); Filipe and Tsiotras (2013a,b); Filipe, Kontitsis and Tsiotras (2015)]. In the end, a brief summary of the aforementioned models are made and discussed in Section 2.6.

2.1 Model overview

The model of the chaser satellite and the uncooperative target is the same as the one in Hou et al. [Hou, Ma, Wang et al. (2017)]. As can been seen in Fig. 1, the inertial frame is represented as {I}, and the center of the Earth is set as the origin of the coordinate. The target's body frame is represented as {B} with the origin at the target's center of mass. In addition, the capturing fixture of the target sets up the coordinate {B'}, which has the same orientation as {B}. As a result, the coordinates {B} and {B'} only have translational distance ρ.

Using the aforementioned model, unit quaternion $q_{B/I}$ is utilized to depict the the rotation of {B} with respect to {I}. $r_{B/I}$ is defined as the distance between the origin of {B} and {I}. In addition, r_m represents the distance between the origin of {B'} and {I}. For the motion part, ω represents the angular velocity of the target with respect to {I} along with v representing the linear velocity of the target with respect to {I}.

2.2 Model kinematics based on traditional quaternions

As proposed in Aghili [Aghili (2012)], the model kinematics based on traditional quaternions can be shown as:

$$\dot{q}_{B/I} = \frac{1}{2}\Omega(\omega^B_{B/I})q_{B/I} \tag{1}$$

where $q_{B/I} = \begin{pmatrix} q_{B/I,0} & \overline{q}_{B/I} \end{pmatrix}$, $\overline{q}_{B/I} = \begin{pmatrix} q_{B/I,1} & q_{B/I,2} & q_{B/I,3} \end{pmatrix}$;
$\omega^B_{B/I} = \begin{pmatrix} \omega^B_{B/I,x} & \omega^B_{B/I,y} & \omega^B_{B/I,z} \end{pmatrix}$; $\Omega(\omega^B_{B/I}) = \begin{bmatrix} 0 & -\omega^B_{B/I,z} & \omega^B_{B/I,y} \\ \omega^B_{B/I,z} & 0 & -\omega^B_{B/I,x} \\ -\omega^B_{B/I,y} & \omega^B_{B/I,x} & 0 \end{bmatrix}$.
Since only 3 out of 4 elements of one set of quaternions can also be utilized to represent the model kinematics, and the singularity problem only happens when the error attitude becomes to 180 degree. The model kinematics based on traditional error quaternions can be represented as [Lefferts, Markley and Shuster (1982)]:

$$\frac{d\delta\overline{q}_{B/I}}{dt} = -\frac{1}{2}\Omega(\omega^B_{B/I})\delta\overline{q}_{B/I} + \frac{1}{2}\delta\omega^B_{B/I} \tag{2}$$

where $\delta\overline{q}_{B/I} = \hat{\overline{q}}^*_{B/I}\overline{q}_{B/I}$, and $\hat{\overline{q}}^*_{B/I}$ is the conjugate of the estimation of $\overline{q}_{B/I}$, and $\delta\overline{q}_{B/I}$ is the error quaternions of $\{\mathrm{B}\}$ with respect to $\{\mathrm{I}\}$.

In Eq. (2), when the error quaternions becomes 180 degrees, the singularity problem occurs. However, as mentioned in Hou et al. [Hou, Ma, Wang et al. (2017)], when utilizing the error quaternions to represent the attitude and the estimations are available, the error attitudes are assumed to be much less than 180 degrees. As a result, by utilizing Eq. (2), the attitude parameters can be estimated without singularity problems.

2.3 Traditional model kinematics and dynamics

The traditional model dynamics without any disturbance and control torques can be represented as follows [Aghili (2012)]:

$$\frac{d\omega^B_{B/I}}{dt} = J^{-1}(-\omega^B_{B/I} \times (J\omega^B_{B/I})) \tag{3}$$

where $J = \begin{bmatrix} J_x & 0 & 0 \\ 0 & J_y & 0 \\ 0 & 0 & J_z \end{bmatrix}$ is the matrix of the inertia tensors of the target.
Combining Eqs. (2) and (3), one can obtain the traditional model kinematics and dynamics equations.

2.4 DVQ based model kinematics

From the Eqs. (2) and (3), it can be found that the position parameters cannot be shown in the traditional models. This phenomenon will lead to a lack of parameter estimation of these position parameters. Also, since the lack of position parameters, the translational and rotational coupled effects are neglected, which will lead to inaccurate system modeling. As a consequence, considering the drawbacks of the parameter estimations using traditional model kinematics and dynamics equations, dual quaternions are utilized in this section to represent the model kinematics. As proposed in Hou et al. [Hou, Ma, Wang et al. (2017); Filipe, Kontitsis and Tsiotras (2015)], the dual quaternions based model kinematics can be represented as follows:

$$2\dot{\hat{q}} = \hat{\omega}^{I}_{B/I}\hat{q}_{B/I} = \hat{q}_{B/I}\hat{\omega}^{B}_{B/I} \tag{4}$$

where $\hat{q}_{B/I} = q_{B/I} + \varepsilon q^{'}_{B/I} = q_{B/I} + \varepsilon\frac{1}{2}q_{B/I}r^{B}_{B/I} = q_{B/I} + \varepsilon\frac{1}{2}r^{I}_{B/I}q_{B/I}$ is the unit dual quaternions from {I} to {B}.
$r^{Z}_{X/Y} = \begin{pmatrix} 0 & \overline{r}^{Z}_{X/Y} \end{pmatrix}$, and $\overline{r}^{Z}_{X/Y} = \begin{pmatrix} \overline{r}^{Z}_{X/Y,x} & \overline{r}^{Z}_{X/Y,y} & \overline{r}^{Z}_{X/Y,z} \end{pmatrix}$ represents the distance of {X} with respect to {Y} expressed in {Z} in quaternion format. $\hat{\omega}^{B}_{B/I} = \omega^{B}_{B/I} + \varepsilon\omega'^{B}_{B/I} = \omega^{B}_{B/I} + \varepsilon v^{B}_{B/I} = \omega + \varepsilon v$ is the motion dual quaternions of {B} with respect to {I} expressed in {B} frame. $\omega^{B}_{B/I} = \begin{pmatrix} 0 & \overline{\omega}^{B}_{B/I} \end{pmatrix}$, and $\overline{\omega}^{B}_{B/I} = \begin{pmatrix} \overline{\omega}^{B}_{B/I,x} & \overline{\omega}^{B}_{B/I,y} & \overline{\omega}^{B}_{B/I,z} \end{pmatrix}$ is the angular velocity of {B} with respect to {I} expressed in {B}. $v^{B}_{B/I} = \begin{pmatrix} 0 & \overline{v}^{B}_{B/I} \end{pmatrix}$, and $\overline{v}^{B}_{B/I} = \begin{pmatrix} \overline{v}^{B}_{B/I,x} & \overline{v}^{B}_{B/I,y} & \overline{v}^{B}_{B/I,z} \end{pmatrix}$ represents the linear velocity of {B} with respect to {I} expressed in {B}. The dual quaternions calculation lemmas can be found in Hou et al. [Hou, Ma, Wang et al. (2017); Filipe, Kontitsis and Tsiotras (2015)].

Similar to the error quaternions based traditional kinematics Eq. (2) , error quaternions of $q_{B/I}$ can also be utilized to decrease the dimensions of the dual quaternions. By using the error attitude quaternions and the vector parts of the other parameters, the DVQ based model kinematics can be represented as [Hou, Ma, Wang et al. (2017); Filipe, Kontitsis and Tsiotras (2015)]:

$$\frac{d\delta\overline{\hat{q}}_{B/I}}{dt} = -\frac{1}{2}\overline{\tilde{\omega}}^{B}_{B/I}\delta\overline{\hat{q}}_{B/I} + \frac{1}{2}\delta\overline{\hat{q}}_{B/I}\overline{\hat{\omega}}^{B}_{B/I} \tag{5}$$

where $\overline{\tilde{\omega}}^{B}_{B/I}$ represents the estimation of $\overline{\omega}^{B}_{B/I}$, $\delta\overline{\hat{q}}_{B/I}$ represents the dual error quaternion. As proposed in Hou et al. [Hou, Ma, Wang et al. (2017)], Eq. (5) only needs to compute 6 dimensions dual vector quaternions instead of the 8 dimensions ones in Filipe et al. [Filipe and Tsiotras (2013a,b); Filipe, Kontitsis and Tsiotras (2015)]. This advantage leads to a 6×6 instead of 8×8 covariance matrix calculation in the estimating procedure for each parameter which can reduce a lot of computational load when there are many parameters to be estimated.

2.5 DVQ based model kinematics and dynamics

The dual quaternions based model dynamics without any disturbance and control torques can be represented as follows [Hou, Ma, Wang et al. (2017); Filipe, Kontitsis and Tsiotras (2015)]:

$$\frac{d(\hat{\omega}_{B/I}^{B})^{s}}{dt} = A^{-1} \otimes (-\hat{\omega}_{B/I}^{B} \times (A \otimes (\hat{\omega}_{B/I}^{B})^{s})) \tag{6}$$

where $A = \begin{bmatrix} A_{11} & A_{12} \\ A_{21} & A_{22} \end{bmatrix}$, $A_{11} = \begin{bmatrix} 0 & 0_{1\times3} \\ 0_{3\times1} & mI_{3\times3} \end{bmatrix}$, $A_{12} = 0_{4\times4}$, $A_{21} = 0_{4\times4}$, $A_{22} = \begin{bmatrix} 0 & 0_{1\times3} \\ 0_{3\times1} & \overline{J_B} \end{bmatrix}$ m is the mass of the target, and $\overline{J_B} = \begin{bmatrix} J_{Bx} & 0 & 0 \\ 0 & J_{By} & 0 \\ 0 & 0 & J_{Bz} \end{bmatrix}$.

The define of the calculation "$\otimes$" can be found in Hou et al. [Hou, Ma, Wang et al. (2017)] and also represented here as:

$$A \otimes \hat{a} = (A_{11}a + A_{12}a^{'}) + \varepsilon(A_{21}a + A_{22}a^{'}) \tag{7}$$

where $\hat{a} = a + \varepsilon a'$, $A = \begin{bmatrix} A_{11} & A_{12} \\ A_{21} & A_{22} \end{bmatrix}$, A_{11},A_{12},A_{21},$A_{22} \in R^{4\times4}$.

By extracting the vector parts of each parameter in Eq. (6) and using the DVQ format to represent Eq. (6), one can obtain the DVQ based model dynamics equations [Hou, Ma, Wang et al. (2017)]:

$$\frac{d(\overline{\hat{\omega}}_{B/I}^{B})^{s}}{dt} = \overline{A}^{-1} \otimes (-\overline{\hat{\omega}}_{B/I}^{B} \times (\overline{A} \otimes (\overline{\hat{\omega}}_{B/I}^{B})^{s})) \tag{8}$$

where $\overline{A} = \begin{bmatrix} \overline{A_{11}} & \overline{A_{12}} \\ \overline{A_{21}} & \overline{A_{22}} \end{bmatrix}$, $\overline{A_{11}} = mI_{3\times3}$, $\overline{A_{12}} = 0_{3\times3}$, $\overline{A_{21}} = 0_{3\times3}$, $\overline{A_{22}} = \overline{J_B}$.

Combining Eq. (5) and Eq. (8), one can obtain the DVQ based model kinematics and dynamics equations.

2.6 Summary of the model kinematics and dynamics

There are four kinds of model kinematics and dynamics equations (which can be divided to two kinds of kinematics and dynamics models) are proposed in this section. Section 2.2 and Section 2.3 give the traditional kinematics and dynamics model which are widely used in various research. However, since the chaser and target are operating in close range, the target and the service satellite cannot be regarded as the point of mass. As a result, the translational and rotational coupled effects should be taken into consideration if one needs to obtain high precision estimations. Comparing Eqs. (2) and (3), it is obvious that the traditional model kinematics and dynamics equations contain the attitude parameters and

the parameters of the inertia tensors. However, it can also be seen that the parameters of the inertia tensors in Eq. (3) is dependent on the attitude parameters in Eq. (2). This is a strong drawback of the parameters estimating using traditional model kinematics and dynamics equations since the parameters of the inertia tensors must be estimated after the attitude parameters converges. This feature leads to a separated parameters estimating action when using the traditional model kinematics and dynamics equations, which will consume much more parameters estimating time [Hou, Ma, Wang et al. (2017); Xing, Cao, Zhang et al. (2010); Filipe and Tsiotras (2013b)]. Also, from the above Eqs. (2) and (3), no parameters of the translational parameters are represented. This is another strong drawback of the parameters estimating using traditional model kinematics and dynamics equations since the very important translational parameters cannot be estimated [Hou, Ma, Wang et al. (2017); Filipe and Tsiotras (2013b)].

Section 2.4 and Section 2.5 give the DVQ based model kinematics and dynamics model. It can be found that Eqs. (5) and (8) contain both of the translational and rotational parameters. Compared to Eqs. (2) and (3), Eqs. (5) and (8) considered the translational and rotational coupled effects and made the attitude and position parameters integrated estimations become possible. In addition, the format of Eqs. (5) and (8) are quite familiar with the well-known Eqs. (2) and (3), and this is another appealing characteristic [Filipe and Tsiotras (2013a,b); Filipe, Kontitsis and Tsiotras (2015)].

Also, it is apparent that Eq. (8) contains the parameters of the inertial tensors of the target. This reveals that the DVQ based model kinematics and dynamics equations can estimate both the pose parameters and the inertial tensors when compared to the DVQ based model kinematics equations. As a result, the DVQ based model kinematics and dynamics equations is the most advanced one among the four kinds of modeling techniques. However, the computational load of it is also the most burdensome.

3 Parameter estimations based on Extended Kalman Filter

The Extended Kalman Filter (EKF) has proved its worth on a multitude of spacecraft missions since it has been proposed [Crassidis, Markley and Yang (2007)]. By using the first order Taylor series expansion method to linearize the state equations, the EKF can be utilized to the nonlinear systems. Although there will be linearization errors in the EKF, this estimation method is still the workhorse of all the other nonlinear estimating techniques [Crassidis, Markley and Yang (2007)]. Also, by calculating and analyzing the Jacobian matrices of the relative systems, the derivatives of the states of each system can be shown analytically and the inner factors (i.e., the derivatives of each parameter with the other state, the relationship between one parameter and the other ones, etc.) that influence the states can be revealed as well [Chaves-Jiménez, Guo and Gill (2017)]. This section firstly proposed the observation models of the LIDAR system. Then, two kinds of EKF based parameters estimating algorithms are designed and each of the two algorithms aims at one kind of the aforementioned system model. Finally, a brief summary is made.

3.1 Observation equations

The LIDAR system is the most widely used sensor in the Autonomous Rendezvous and Docking (AR&D) scenarios for it is robust to the complex lighting environment of the space and can provide the pose measurements. The relative attitude and distance of the grapple fixture can be measured as:

$$Y = \begin{bmatrix} q_m \\ r_m \end{bmatrix} + v \tag{9}$$

where r_m represents distance between {B'} and {I}. q_m represents the relative attitude between {B'} and {I}. v is the noise of the measurements with a covariance matrix $R = E[vv^T]$.

Define the state vector of the system for the traditional kinematics and dynamics equations (Section 2.2 and Section 2.3) as:

$$X_1 = [\ \overline{q}_{B/I} \quad \omega^B_{B/I} \quad p \quad \rho\ ] \tag{10}$$

where $p = [\ p_x \quad p_y \quad p_z\ ]$ is the moments of inertia ratios of the target, which is defined as the same as the one in Aghili [Aghili (2012)]:
$p = \left[\ p_x = \frac{J_{By}-J_{Bz}}{J_{Bx}} \quad p_y = \frac{J_{Bz}-J_{Bz}}{J_{By}} \quad p_x = \frac{J_{Bx}-J_{By}}{J_{Bz}}\ \right]$, $\rho = [\ \rho_x \quad \rho_y \quad \rho_z\ ]$ depicts the distance between center of mass and the capturing fixture.

Define the state vector of the system for the DVQ based kinematics and dynamics equations (Section 2.4 and Section 2.5) as:

$$X_2 = [\ \overline{\hat{q}}_{B/I} \quad \overline{\hat{\omega}}^B_{B/I} \quad \overline{\hat{p}} \quad \overline{\hat{\rho}}\ ] \tag{11}$$

where $\overline{\hat{q}}_{B/I}$ is the vector part of $\hat{q}_{B/I}$, $\overline{\hat{\omega}}_{B/I}$ is the vector part of $\hat{\omega}_{B/I}$, $\overline{\hat{p}}$ is the vector part of $\hat{p}$, $\hat{p} = p + \varepsilon 0$, $p = [\ 0 \quad p_x \quad p_y \quad p_z\ ]$ is the moments of inertia ratios of the target, and defining as the same as the one in Aghili [Aghili (2012)]:
$p = \left[\ p_x = \frac{J_{By}-J_{Bz}}{J_{Bx}} \quad p_y = \frac{J_{Bz}-J_{Bz}}{J_{By}} \quad p_x = \frac{J_{Bx}-J_{By}}{J_{Bz}}\ \right]$, $\overline{\hat{\rho}}$ is the vector part of $\hat{\rho}$, $\hat{\rho} = \rho + \varepsilon 0$ depicts the distance between center of mass and the capturing fixture in quaternion form.

Using the same linearizing technique in Hou et al. [Hou, Ma, Wang et al. (2017)], the observation equations can be represented as:

$$\begin{aligned} Y_1 &= y(X_1) + v \\ &= \begin{bmatrix} \tilde{q}_{B/I} + Q(\tilde{q}_{B/I})\delta q_{B/I} \\ \overline{r}^I_{B/I} + [A(\tilde{q}_{B/I})(I_{3\times 3} + 2[\delta \overline{q}_{B/I}\times])]\rho \end{bmatrix} + v \end{aligned} \tag{12}$$

$$\begin{aligned} Y_2 &= y(X_2) + v \\ &= \begin{bmatrix} \tilde{q}_{B/I} + Q(\tilde{q}_{B/I})\delta q_{B/I} \\ Y_{21} + [A(\tilde{q}_{B/I})(I_{3\times 3} + 2[\delta \overline{q}_{B/I}\times])]\overline{\rho} \end{bmatrix} + v \end{aligned} \tag{13}$$

where

$$Y_{21} = 2(\bar{\tilde{q}}_{B/I}\delta\bar{\tilde{q}}_{B/I})'\bar{q}^*_{B/I}\delta\bar{\tilde{q}}_{B/I} \tag{14}$$

3.2 Extended Kalman filter based on kinematics and dynamics in traditional quaternions form

In this situation, define the state vector of the system as:

$$X_1 = [\ \bar{q}_{B/I} \quad \omega^B_{B/I} \quad p \quad \rho\ ] \tag{15}$$

Since the unit quaternions have the relationship: $q^2_{B/I,0} + q^2_{B/I,1} + q^2_{B/I,2} + q^2_{B/I,3} = 1$, using only three out of four elements of one set of unit quaternions can represent the relative attitude. Therefore, in the selected states, only the vector part of the full unit quaternions is chosen.

By the selected state Eq. (15) and using the same linearizing technique in Hou et al. [Hou, Ma, Wang et al. (2017)], one can linearize observation equation as:

$$\begin{aligned} H_1(X_1) &= \tfrac{\partial y(X_1)}{\partial X_1} \\ &= \begin{bmatrix} Q(\tilde{q}_{B/I}) & 0_{3\times3} & 0_{3\times3} & 0_{3\times3} \\ -2A(\tilde{q}_{B/I})\,[\overline{\rho}\times] & 0_{3\times3} & 0_{3\times3} & H_{11} \end{bmatrix} \end{aligned} \tag{16}$$

where

$$H_{11} = A(\tilde{q}_{B/I}) + 2A(\tilde{q}_{B/I})(\delta\overline{q}_{B/I}\times) \tag{17}$$

Assuming that the proportions of the inertial tensors of the target are constants and the uncooperative space target is a rigid body, define:

$$\dot{p} = [\ 0 \quad 0 \quad 0\ ]^T \tag{18}$$

$$\dot{\rho} = [\ 0 \quad 0 \quad 0\ ]^T \tag{19}$$

Using the same linearizing technique in Hou et al. [Hou, Ma, Wang et al. (2017)], the linearization form of the state equations can be represented as:

$$X_{1,k} = \Phi_{1,k/k-1}X_{1,k-1} \tag{20}$$

where $\Phi_{1,k+1/k} = e^{F_{1,k}T} \doteq I + F_{1,k}T$, $F_{1,k} = \begin{bmatrix} -(\omega^B_{B/I}\times) & \frac{1}{2}I_{3\times3} & 0_{3\times3} & 0_{3\times3} \\ 0_{3\times3} & A_1 & B_1 & 0_{3\times3} \\ 0_{3\times3} & 0_{3\times3} & 0_{3\times3} & 0_{3\times3} \\ 0_{3\times3} & 0_{3\times3} & 0_{3\times3} & 0_{3\times3} \end{bmatrix}$,

$A_1 = \begin{bmatrix} 0 & p_x\omega_z & p_x\omega_y \\ p_y\omega_z & 0 & p_y\omega_x \\ p_z\omega_y & p_z\omega_x & 0 \end{bmatrix}$, $B_1 = \begin{bmatrix} \omega_y\omega_z & 0 & 0 \\ 0 & \omega_x\omega_z & 0 \\ 0 & 0 & \omega_x\omega_y \end{bmatrix}$, T is the time interval between sampling points.

Furthermore, the covariance of the discrete-time process can be calculated as:

$$Q_{1,k} = C_{1,k} D_{1,k}^{-1} \tag{21}$$

where $\begin{pmatrix} C_{1,k} \\ D_{1,k} \end{pmatrix} = \exp\left\{ \begin{pmatrix} F_{1,k} & Q_{1,c} \\ 0 & -F_{1,k}^T \end{pmatrix} T \right\} \begin{pmatrix} 0 \\ I \end{pmatrix}$,
$Q_{1,c} = diag\{ \ 0_{3\times3} \quad \sigma_1^2 \quad 0_{3\times3} \quad 0_{3\times3} \ \}$, and σ_1 is the standard deviation of the processing noise.

Depending on the aforementioned analysis, the EKF based on traditional quaternions based kinematics and dynamics model can be represented as:

$$\delta X_{1,k/k-1} = \Phi_{1,k/k-1} \delta X_{1,k-1/k-1} \tag{22}$$

$$X_{1,k/k-1} = X_{1,k-1/k-1} + \delta X_{1,k/k-1} \delta T \tag{23}$$

$$P_{1,k/k-1} = \Phi_{1,k/k-1} P_{1,k-1/k-1} \Phi_{1,k/k-1}^T + Q_{1,k} \tag{24}$$

$$K_{1,k} = P_{1,k/k-1} H_{1,k}^T (H_{1,k} P_{1,k/k-1} H_{1,k}^T + R_k)^{-1} \tag{25}$$

$$\delta X_{1,k} = K_{1,k} (Y_{1,k} - y_1(X_{1,k/k-1})) \tag{26}$$

$$P_{1,k} = [I - K_{1,k} H_{1,k}] P_{1,k/k-1} \tag{27}$$

To update the quaternions, the following equation is utilized:

$$q_{B/I,k} = q_{B/I,k-1} \delta q_{B/I,k} \tag{28}$$

where $\delta q_{B/I,k} = (\ \sqrt{1 - \left\| \delta \overline{q}_{B/I,k} \right\|^2} \quad \delta \overline{q}_{B/I,k} \ )$.
To update the other states, using the following equation:

$$X_{1,k/k} = X_{1,k-1/k-1} + \delta X_{1,k} \tag{29}$$

3.3 Extended Kalman filter based on DVQ based kinematics and dynamics model

In this situation, define the state vector of the system as:

$$X_2 = [\ \overline{\hat{q}}_{B/I} \quad \overline{\hat{\omega}}_{B/I}^B \quad \overline{\hat{p}} \quad \overline{\hat{\rho}} \ ] \tag{30}$$

By the selected state Eq. (30) and using the same technique in Hou et al. [Hou, Ma, Wang et al. (2017)], the linearization format of $y(X_2)$ can be represented as:

$$\begin{aligned} H_2(X_2) &= \frac{\partial y(X_2)}{\partial X_2} \\ &= \begin{bmatrix} Q(\tilde{q}_{B/I}) & 0_{4\times3} & 0_{4\times6} & 0_{4\times6} & 0_{4\times6} \\ -2A(\tilde{q}_{B/I}) [\overline{\rho}\times] & \Gamma(\tilde{q}_{B/I}) & 0_{3\times6} & 0_{3\times9} & H_{22} \end{bmatrix} \end{aligned} \tag{31}$$

where $\Gamma(\tilde{q}_{B/I}) = 2(\bar{\tilde{\hat{q}}}_{B/I})' \delta\bar{\tilde{q}}_{B/I}\bar{\tilde{q}}^*_{B/I} = 2A(\tilde{q}_{B/I}), H_{22} = A(\tilde{q}_{B/I}) + 2A(\tilde{q}_{B/I})(\delta\overline{q}_{B/I}\times)$. Since the proportions of the inertial tensors are constants and the uncooperative space target is a rigid body, it can be discovered that:

$$\dot{\bar{\hat{p}}} = \bar{\hat{0}} \tag{32}$$

$$\dot{\bar{\hat{\rho}}} = \bar{\hat{0}} \tag{33}$$

Using the same technique in Hou et al. [Hou, Ma, Wang et al. (2017)], the linearization form of the state equations can be represented as:

$$X_{2,k+1} = \Phi_{2,k/k-1}X_{2,k} + w_k \tag{34}$$

where $\Phi_{2,k/k-1} = e^{F_{2,k}\triangle T} \doteq I + F_{2,k}\Delta T$, $F_{2,k} = \begin{bmatrix} -(\bar{\tilde{\omega}}^B_{B/I}\times) & \frac{1}{2}I_{6\times6} & 0_{6\times6} & 0_{6\times6} \\ 0_{6\times6} & A_2 & B_2 & 0_{6\times6} \\ 0_{6\times6} & 0_{6\times6} & 0_{6\times6} & 0_{6\times6} \\ 0_{6\times6} & 0_{6\times6} & 0_{6\times6} & 0_{6\times6} \end{bmatrix}$, $A_2 = \begin{bmatrix} A_{21} & A_{22} \\ (v\times) & -(\omega\times) \end{bmatrix}$, $A_{21} = \begin{bmatrix} 0 & p_x\omega_z & p_x\omega_y \\ p_y\omega_z & 0 & p_y\omega_x \\ p_z\omega_y & p_z\omega_x & 0 \end{bmatrix}$, $A_{22} = 0_{3\times3}$,

$B_2 = \begin{bmatrix} B_{21} & 0_{3\times3} \\ 0_{3\times3} & 0_{3\times3} \end{bmatrix}$, $B_{21} = \begin{bmatrix} \omega_y\omega_z & 0 & 0 \\ 0 & \omega_x\omega_z & 0 \\ 0 & 0 & \omega_x\omega_y \end{bmatrix}$, $\triangle T$ is the sampling time.

Furthermore, the covariance of the discrete-time process can be calculated as:

$$Q_{2,k} = C_{2,k}D^{-1}_{2,k} \tag{35}$$

where $\begin{pmatrix} C_{2,k} \\ D_{2,k} \end{pmatrix} = \exp\left\{ \begin{pmatrix} F_{2,k} & Q_{2,c} \\ 0 & -F^T_{2,k} \end{pmatrix} T \right\} \begin{pmatrix} 0 \\ I \end{pmatrix}$, and

$Q_{2,c} = diag\{\ 0_{6\times6} \quad \sigma^2_\omega \quad \sigma^2_v \quad 0_{6\times6} \quad 0_{6\times6}\ \}$.

Depending on the aforementioned analysis, the EKF based on DVQ can be represented as

$$\delta X_{2,k/k-1} = \Phi_{2,k/k-1}\delta X_{2,k-1/k-1} \tag{36}$$

$$X_{2,k/k-1} = X_{2,k-1/k-1} + \delta X_{2,k/k-1}\delta T \tag{37}$$

$$P_{2,k/k-1} = \Phi_{2,k/k-1}P_{2,k-1/k-1}\Phi^T_{2,k/k-1} + Q_{2,k} \tag{38}$$

$$K_{2,k} = P_{2,k/k-1}H^T_{2,k}(H_{2,k}P_{2,k/k-1}H^T_{2,k} + R_k)^{-1} \tag{39}$$

$$\delta X_{2,k} = K_{2,k}(Y_{2,k} - y(X_{2,k/k-1})) \tag{40}$$

$$P_{2,k} = [I - K_{2,k}H_{2,k}]P_{2,k/k-1} \tag{41}$$

To update the quaternions, the following equation is utilized:

$$\hat{q}_{B/I,k} = \hat{q}_{B/I,k-1}\delta\hat{q}_{B/I,k} \tag{42}$$

where $\delta\hat{q}_{B/I,k} = \delta q_{B/I,k} + \varepsilon\delta q'_{B/I,k}$, $\delta q_{B/I,k} = \left(\sqrt{1 - \left\|\delta\overline{q}_{B/I,k}\right\|^2} \quad \delta\overline{q}_{B/I,k} \right)$,

$\delta q'_{B/I,k} = \left(\frac{-\delta\overline{q}_{B/I,k}\delta\overline{q'}^{*}_{B/I,k}}{\sqrt{1-\left\|\delta\overline{q}_{B/I,k}\right\|^2}} \quad \delta\overline{q'}_{B/I,k} \right)$

To update the other states, using the following equation:

$$X_{2,k/k} = X_{2,k-1/k-1} + \delta X_{2,k} \tag{43}$$

3.4 Summary of the EKFs with different models

This section proposes two kinds of EKF based parameters estimation algorithms based on the aforementioned models along with the observation equations provided by LIDAR systems. Firstly, the observation equations of the LIDAR systems are given and the linearization of them are derived. Then, the EKF based on the kinematic and dynamics model in traditional quaternions form and the DVQ-EKF are proposed. From the two kinds of EKFs, it can be found that the DVQ-EKF can estimate not only the attitude parameters and inertial parameters but also the translational parameters as well when compared to the EKF based on the kinematic and dynamics model in traditional quaternions form. As a result, by considering the coupling effects between the translation and rotation, the DVQ-EKF can be considered as the "full parameters" estimation algorithm without contacting the uncooperative space target [Hou, Ma, Wang et al. (2017)].

4 Observability determination

The OG is computed in this section. By computing the rank of the observability matrix, whether the EKFs with traditional modeling technique and DVQ modeling technique is observable is discovered. Then, by setting a threshold and calculating the Condition number of each of the aforementioned two systems, the degree of observability by which not only determining whether a system is observable or not but also the degree of observability of a system is computed. Further more, in order to study the Observability matrix more comprehensively, the Singular Value Decomposition (SVD) method is utilized to analyze which combination of the states is the most observable and which one is the least observable [Chaves-Jiménez, Guo and Gill (2017); Ham and Brown (1983)]. Then, the covariance time evolution analysis is made to analyze the observability of each of the two aforementioned systems in the view of estimation covariance. Finally, a brief summary is made.

4.1 Observability matrix

The discrete Observability Gramian (OG) matrix is computed as [Chaves-Jiménez, Guo and Gill (2017)]:

$$OG = \sum_{k=1}^{m} \Phi(t_k, t_0) H_k^T R_k^{-1} H_k \Phi^T(t_k, t_0) \tag{44}$$

where $\Phi(t_k, t_0) = \Phi_{k/k-1} \cdots \Phi_{2/1} \Phi_{1/0}$, and m is the total simulation steps during the parameter estimating procedure.

Depending on different aforementioned models, the OG matrices can be represented as:

1. For the case of traditional quaternions based kinematics and dynamics model:

$$OG_1 = \sum_{k=1}^{m} \Phi_1(t_k, t_0) H_{1,k}^T R_k^{-1} H_{1,k} \Phi_1^T(t_k, t_0) \tag{45}$$

2. For the case of DVQ based kinematics and dynamics model:

$$OG_2 = \sum_{k=1}^{m} \Phi_2(t_k, t_0) H_{2,k}^T R_k^{-1} H_{2,k} \Phi_2^T(t_k, t_0) \tag{46}$$

A system is fully observable means that the states can be recovered from the measurements no matter what the initial values of them are chosen. On the contrary, if a system is not fully observable, the states may be affected by the relative initial values or the states cannot be well estimated. By the OG method, a system is considered fully observable if the rank of the OG matrix has full rank [Krener and Ide (2009)]. By utilizing the OG matrix, one can discover whether a system is fully observable or not during the total simulating time. However, only using the OG matrix cannot show how observable a system is.

Since the observability is analyzed by computer simulations, a tolerance value must be pre-defined to check the rank of the relative OG matrix to account for the numerical error. The tolerance value can be set as [Friedman and Frueh (2018)]:

$$tol = max(\lambda_i) \times max(size(OG_i)) \times eps \tag{47}$$

where λ_i is the singular values of the OG matrix, eps is the machine precision. Since the singular values must be above some tolerance to account for numerical error, only when the singular value of the OG matrix is bigger than tol will it be considered as positive value.

4.2 Observability conditions

Since the rank of the OG matrix cannot indicate the degree of the observability of a certain system, the Condition number of the OG matrix is introduced as a measurement of the degree of observability. The Condition number of a OG matrix is defined as [Yu, Cui and Zhu (2014)]:

$$cond = \frac{max(\lambda_i)}{min(\lambda_i)} \tag{48}$$

where λ_i are the singular values of the OG matrix.

The condition number can reveal the innate characteristics of an OG matrix. If the condition number is big, it shows that the maximum singular value is much bigger than the minimum one. This phenomenon indicates that a small disturbance from the noise can have huge effects on the observability matrix. In this situation, an OG matrix is considered to be ill-conditioned and will provide a lower degree of observability. However, when the condition number is small, it shows that the maximum singular value and the minimum singular value are close. This indicate that the system is well conditioned and has a relatively better observability. As a result, the larger condition number a system has, the lower observability it will be [Chaves-Jiménez, Guo and Gill (2017); Wilson and Guhe (2005); Krener and Ide (2009)].

Also, the inverse of the condition number is selected as a indicator to show the degree of observability of a system [Yu, Cui and Zhu (2014)]:

$$ob = \frac{1}{cond} \tag{49}$$

The bigger ob means the better observability of a system.

By the calculated condition number, one can not only find whether a system is observable or not but also reveal how observable a system is. Nevertheless, the state with the most influence on the observability is still obscure. In the parameters estimating tasks of an unknown space target, it is vital important to find out which state is the most observable and which one is the least. To achieve this goal, the SVD method is utilized. By using the SVD method to an OG matrix, the OG matrix can be represented as:

$$OG = USV^T \tag{50}$$

where S contains the singular values of the relative OG matrix, U and V contain the singular vectors of the OG matrix. Denote u_i and v_i are the column vector relative to λ_i.

After normalization of the OG matrix [Chaves-Jiménez, Guo and Gill (2017); Ham and Brown (1983)], singular values and the relative column vectors can reveal the following characters. The column vector of the maximum singular value of the OG matrix reveals the most observable linear combination of the relative states, and the biggest values (absolute value) in the column vector indicates the most observable states. On the contrary, the minimum singular values of the OG matrix reveals the least observable linear combination of the relative states [Ablin (1967); Ham and Brown (1983)].

4.3 Covariance time evolution analysis

The covariance of the states in each aforementioned models contains all the standard deviations of the parameter estimates. The time evolution analysis of the covariance can

reveal the estimation error of every parameters varying with time. In addition, by using the covariance time evolution analysis, one can discover the final error of a certain parameter and check whether the relative parameter is well estimated. Also, this analysis can be utilized as a tool to test the observability analyzing results. If a parameter has a good observability, the standard deviation of it will convergent to zero. On the contrary, the standard deviation will have error if a parameter is assumed to be with low degree of observability. In other words, the covariance time evolution analysis has strong relationship with the observability analysis. The higher observability a parameter has the lower the covariance error will be and vice versa.

4.4 Summary of the observability determination

This section gives there kinds of approaches to analyze the observabilities of the models in Section 2.3 and Section 2.5 along with the method to compute the observability matrix. First of all, the OG method is calculated by Eq. (45). Then, the rank condition analysis method is introduced to check whether the system is observable or not. Furthermore, by computing the condition number of each observability matrix, the degree of observability of a certain system is revealed. In addition, the most to least observability of the linear combination of the parameters are made by the SVD method. It can be found that the covariance of the measurement noise will affect the observability analyzing results by Eq. (45). Although the values of the R_k are positive, they can change the singular values of the OG matrix that will affect the condition number which in turn affects the observability analyzing results. If a singular value of the OG matrix is quite close to the threshold computed by Eq. (47), the measurement noise may affect it and make it below the threshold which will affect the observability [Chaves-Jiménez, Guo and Gill (2017); Friedman and Frueh (2018); Bageshwar, Gebre-Egziabher, Garrard et al. (2009)]. Finally, the covariance time evolution analysis is made to show the standard deviation varying with time of each parameter to verify the results of the observability analysis.

5 Simulation

The mathematical experiment results are presented in this section. First of all, the simulation initial conditions are given. Then, the rank of each of the two aforementioned models varying with time is shown. In addition, the condition number is analyzed. Furthermore, by utilizing the SVD method, the rank of observability of each parameters in the relative system is depicted. Finally, the covariance of each algorithm is shown and the standard deviations of each parameter varying with time is depicted to test whether the observability analysis are effective.

5.1 Initial conditions

The initial conditions are set as the same as the ones in Hou et al. [Hou, Ma, Wang et al. (2017)] to analyze the intrinsic factors that affect the two EKFs based on different models. The initial conditions of the states are set in Tab. 1.

Table 1: Initial conditions of the states

Variable	Initial value
$q_{B/I}$	$q_{B/I}(0) = (0.5, 0.5, 0.5, 0.5)^T$
$r^I_{B/I}$	$r^I_{B/I}(0) = (0, 55, 55, 55)^T m$
$\omega^B_{B/I}$	$\omega^B_{B/I}(0) = (0, 0.5, 0.5, 0.5)^T rad/s$
$v^B_{B/I}$	$v^B_{B/I}(0) = (0, 0, 0, 0)^T m/s$
p	$p(0) = (0, 1, -1, 0)^T$
ρ	$\rho(0) = (0, 0, 0, 0)^T m$

Table 2: Real initial values of the states

Variable	Initial value
$q_{B/I}, real$	$q_{B/I}, real(0) = (1, 0, 0, 0)^T$
$r^I_{B/I}, real$	$r^I_{B/I}, real(0) = (0, 50, 50, 50)^T m$
$\omega^B_{B/I}, real$	$\omega^B_{B/I}, real(0) = (0, 0.1, 0.1, 0.1)^T rad/s$
$v^B_{B/I}, real$	$v^B_{B/I}, real(0) = (0, 0.01, 0.01, 0.01)^T m/s$
p_{real}	$p_{real}(0) = (0, 3/7, -3/7, 0)^T$
ρ_{real}	$\rho_{real}(0) = (0, 0.5, 0.5, 0.5)^T m$

The real initial values of the states are set in Tab. 2.

In addition, the covariances of the processing noise are set as:

$$\sigma_\omega^2 = 5 \times 10^{-4} (rad/s)^2 \tag{51}$$

$$\sigma_v^2 = 1 \times 10^{-3} (m/s)^2 \tag{52}$$

The frequency of the LIDAR is 2 Hz, and the initial values of measurements are given as:

$$q_{B/I,m}(0) = (0.5, 0.5, 0.5, 0.5)^T \tag{53}$$

and

$$r^I_{B/I,m}(0) = (55, 55, 55)^T m \tag{54}$$

with the covariances of the measurement noise as:

$$R = diag((0.01) I_{4\times4}, (0.1) I_{4\times4}) \tag{55}$$

Furthermore, the initial state covariance matrix can be represented as : $P_1(0) = I_{12\times12}$ and $P_2(0) = I_{24\times24}$. The simulation time is set as: $T_1 = T_2 = T = 300s$.

5.2 Rank of the OG matrix

In this subsection, the rank of the OG matrix of each of the aforementioned two models varying with time will be shown. The OG matrix is calculated by Eqs. (45) and (46), and the threshold is calculated by Eq. (47).

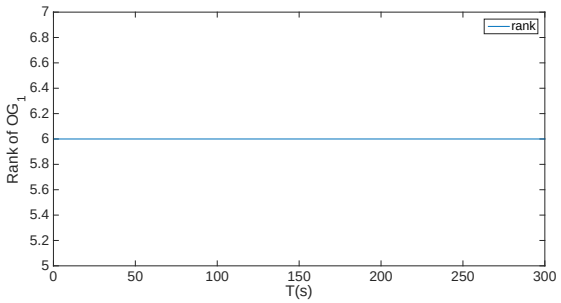

Figure 2: The rank of the OG_1 matrix varying with time

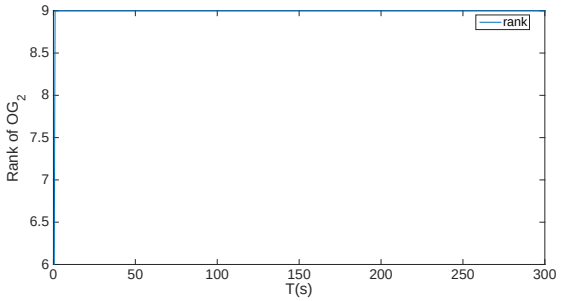

Figure 3: rank of the OG_2 matrix varying with time

It can be seen from Figs. 2 and 3 that the ranks of both of the OG_1 and OG_2 matrices are not full rank. These simulation results reveal that the parameters of the uncooperative space target are not fully observable during the parameters estimating process. In the OG_1 case, the rank converged at 6 soon after the start of the simulation and the rank of the OG_2 becomes 9 instead. Although the rank of the OG_1 case is lower than the one of the OG_2 case, it cannot say that the observability of the traditional quaternions based kinematics and dynamics model is worse than the one of the DVQ based kinematics and dynamics model. From the the aforementioned Section 3.2, the number of parameters to be estimated in the case of traditional quaternions based kinematics and dynamics model is 4 with the dimensions of 12. However, the number of parameters to be estimated in the case of DVQ based kinematics and dynamics model is 6 with the dimensions of 18. As a result, from the rank results it can be reveal that both the traditional quaternions based kinematics and dynamics model and DVQ based kinematics and dynamics model have the same proportions of the rank of the relative OG matrix (33%). Nevertheless, the DVQ based kinematics and dynamics model can be utilized to estimate translational parameters where the traditional quaternions based kinematics and dynamics model fails.

5.3 Observability conditions analysis

From the simulations in Section 5.2, only by utilizing the rank results, the degree of the observabilities cannot be revealed. Figs. 4 and 5 show the conditional number of the

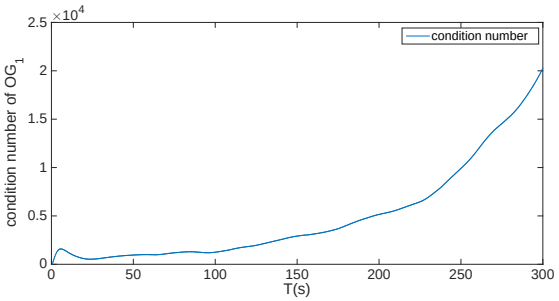

Figure 4: The condition number of the OG_1 matrix varying with time

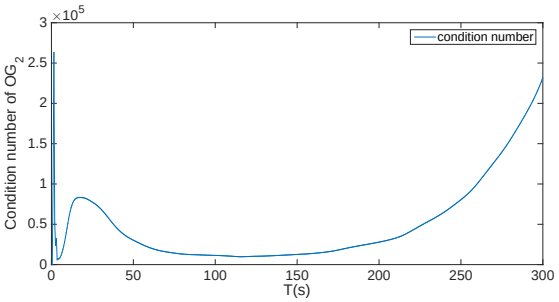

Figure 5: The condition number of the OG_1 matrix varying with time

OG_1 and OG_2 matrices varying with time. Form the simulation results, it can be found that the conditional number of the OG_1 is around 6000 however the one of the OG_2 is much larger. From the aforementioned Section 5.3, if a system has a larger condition number, the degree of observability will be lower. As a result, kinematics and dynamics in traditional quaternions form can provide a better observability when compared to the DVQ based kinematics and dynamics model. The main reason of this phenomenon is that the DVQ based kinematics and dynamics model contains more unobservable parameters although the proportions of the unobservable parameters are the same as the ones in the case of traditional quaternions based kinematics and dynamics model. Since there are more translational parameters to be estimated by the estimating algorithms using DVQ based kinematics and dynamics model, the degree of observability of OG_2 is lower. This can be regarded as the cost of estimating the translational parameters.

5.4 OG matrices SVD analysis

From the above two kinds of analysis, whether a system is observable and how observable the system is are discovered. However, which parameter in the relative system is the most observable one and which one is the least observable are still obscure. As introduced by Yu et al. [Yu, Cui and Zhu (2014)], the SVD method is utilized to find out the ranks of the parameters estimated.

Since the OG_1 and OG_2 are both not with full rank, the ranks of the parameters estimated

Table 3: Tab. 2. SVD results of the OG_1 (EKF based on traditional quaternions based kinematics and dynamics model)

singular values	1.17×10^8	1.16×10^8	1.8×10^6	6×10^3	5.9×10^3	$v_6 = 5.8 \times 10^3$
Column vector	V_1	V_2	V_3	V_4	V_5	V_6
$q_{B/I,1}$	-0.4162	**0.6996**	-0.5808	5.3×10^{-5}	-4.9×10^{-5}	7×10^{-5}
$q_{B/I,2}$	$\mathbf{-0.8371}$	-0.5442	-0.0556	3.36×10^{-5}	0.0001	-0.0008
$q_{B/I,3}$	0.3550	-0.4630	$\mathbf{-0.8121}$	-2.24×10^{-5}	-0.0002	-0.0088
$\omega^B_{B/I,x}$	0	0	0	2.2×10^{-5}	3.37×10^{-5}	0
$\omega^B_{B/I,y}$	0	0	0	1.9×10^{-5}	0	0
$\omega^B_{B/I,z}$	0	0	0	0	0	0
p_1	0	0	0	0	0	0
p_2	0	0	0	0	0	0
p_3	0	0	0	0	0	0
ρ_x	0.0002	8.84×10^{-5}	0.0036	0.6467	$\mathbf{0.6831}$	-0.3392
ρ_y	1.09×10^{-5}	0.0002	0.0091	0.1142	-0.5264	$\mathbf{-0.8425}$
ρ_z	-0.0102	9.2×10^{-5}	-0.0045	$\mathbf{0.7541}$	-0.5062	0.4185

are only focus on the singular values that exceed the threshold by Eq. (47).

Tab. 3 reveals the SVD results of the case of using traditional quaternions based kinematics and dynamics model. It can be found that in Tab. 2, only 6 parameters are observable and the rank of the observability of the estimated parameters is: $q_{B/I,2} > q_{B/I,1} > q_{B/I,3} > \rho_z > \rho_x > \rho_y$. $\omega^B_{B/I,x}, \omega^B_{B/I,y}, \omega^B_{B/I,z}, p, p_2, p_3$ are not observable.

Tab. 4 reveals the SVD results of the case of using the DVQ based kinematics and dynamics model. It can be found that in Tab. 4, only 9 parameters are observable and the rank of the observability of the estimated parameters is : $r^I_{B/I,z} > r^I_{B/I,x} > r^I_{B/I,y} > q_{B/I,3} > q_{B/I,1} > q_{B/I,2} > \rho_z > \rho_x > \rho_y$. $\omega^B_{B/I,x}, \omega^B_{B/I,y}, \omega^B_{B/I,z}, v^B_{B/I,x}, v^B_{B/I,y}, v^B_{B/I,z}, p_1, p_2, p_3$ are not observable.

As the singular values reveal the abilities of enlarging or shrinking a vector by a certain matrix, the singular values of OG_1 and OG_2 can reveal which state is the most accurately estimated one. The biggest value of a state in the column vector of the largest singular value represent the most observable state, and the singular values of the same state in the relative column vector of OG_1 and OG_2 represent which one has the higher estimating accuracy. As seen in Tabs. 3 and 4, the state $q_{B/I,1}, q_{B/I,2}, q_{B/I,3}$ have the singular values of $1.17 \times 10^8, 1.16 \times 10^8, 1.8 \times 10^6$ in OG_1 and $0.001 \times 10^9, 0.006 \times 10^9, 0.005 \times 10^9$ in OG_2 respectively. Since the singular values of the same states in OG_2 is smaller than the ones in OG_1, the parameters $q_{B/I,1}, q_{B/I,2}, q_{B/I,3}$ have higher estimating accuracies when utilizing the traditional quaternions based kinematics and dynamics model. For the other three common states ρ_x, ρ_y, ρ_z, the relative singular values are almost the same, which will lead to similar estimating accuracies. This phenomenon shows that kinematics and dynamics in traditional quaternions form will have higher accuracies when utilized in estimating the relative attitudes. This is quite understandable since the kinematics and dynamics in traditional quaternions form has less parameters to estimate (which leads to lower nonlinearities in estimation) and the traditional quaternions based kinematics and dynamics model neglect the translational and rotational coupled effects that will make the

Table 4: SVD results of the OG_2 (EKF based onDVQ based kinematics and dynamics model)

Singular values	1.367×10^9	1.041×10^9	6×10^8	1×10^6	6×10^6	5×10^6	5.99×10^3	5.97×10^3	5.90×10^3
Column vector	V_1	V_2	V_3	V_4	V_5	V_6	V_7	V_8	V_9
$q_{B/I,1}$	-0.0157	0.0017	-0.0109	0.0545	$\mathbf{-0.8106}$	-0.5826	-0.0003	0.0014	-0.0106
$q_{B/I,2}$	-0.0007	0.0133	0.0118	-0.2690	0.5499	$\mathbf{-0.7905}$	-0.0003	-0.0057	-0.0024
$q_{B/I,3}$	-0.0001	-0.0152	-0.0106	$\mathbf{-0.9615}$	-0.1996	0.1880	0.0008	0.0009	-0.0049
$q_{d,B/I,1}(r^I_{B/I,x})$	0.0838	$\mathbf{-0.9227}$	-0.3754	0.0127	0.0138	-0.0159	-2.6×10^{-6}	-0.0002	4×10^{-5}
$q_{d,B/I,2}(r^I_{B/I,y})$	-0.4330	0.3058	$\mathbf{-0.8478}$	0.0018	0.0174	0.0044	2.8×10^{-5}	-0.0001	0.0003
$q_{d,B/I,3}(r^I_{B/I,z})$	$\mathbf{0.8974}$	0.2338	-0.3741	0.0003	-0.0666	-0.0072	1.4×10^{-5}	2×10^{-6}	-0.0001
$\omega^B_{B/I,x}$	0	0	0	0	0	0	0	0	0
$\omega^B_{B/I,y}$	0	0	0	0	0	0	0	0	0
$\omega^B_{B/I,z}$	0	0	0	0	0	0	0	0	0
$v^B_{B/I,x}$	0	0	0	0	0	0	0	0	0
$v^B_{B/I,y}$	0	0	0	0	0	0	0	0	0
$v^B_{B/I,z}$	0	0	0	0	0	0	0	0	0
p_1	0	0	0	0	0	0	0	0	0
p_2	0	0	0	0	0	0	0	0	0
p_3	0	0	0	0	0	0	0	0	0
ρ_x	-2.4×10^{-5}	-1.15×10^{-5}	-3.3×10^{-5}	0.0025	0.0668	0.0012	0.6457	0.5584	-0.5209
ρ_y	2.85×10^{-5}	-8×10^{-5}	-1.3×10^{-6}	-0.0028	0.0004	-0.0058	-0.4011	$\mathbf{0.8284}$	0.3909
ρ_z	-3.25×10^{-5}	3.59×10^{-5}	-0.0001	0.0031	0.0064	0.0056	$\mathbf{-0.6498}$	0.0435	$\mathbf{-0.7588}$

attitude estimation much easier. The further simulations of the estimating accuracies of every parameter will be shown in the following subsection Section 5.5.

Furthermore, from the above Tabs. 3 and 4, it can be revealed that the parameters relative to the measurements are with higher degree of observabilities (q, r and ρ), and the dynamic parameters (ω and v) and inertial parameters (p) are not observable. In addition, the parameters estimated by the traditional quaternions based kinematics and dynamics model are with higher observability than the same ones estimated by DVQ based kinematics and dynamics model. This phenomenon o shows that the DVQ based kinematics and dynamics model is sensitive to the initial conditions compared to the traditional quaternions based kinematics and dynamics model since there are more unobservable parameters to estimate.

5.5 Covariance time evolution analysis

Figs. 6 and 7 show the norm of the covariances of the estimation results using traditional quaternions based kinematics and dynamics model and the estimation results using DVQ based kinematics and dynamics model separately. It can be found that the final norm of the covariance of the DVQ based EKF is higher since the DVQ-EKF has more observable states. However, the estimation results using traditional quaternions based kinematics and dynamics model has less initial fluctuations which proved the aforementioned analysis.

Fig. 8 to Fig. 17 show the standard deviations of the parameters estimated using both of the two models.It can be found in Figs. 8 and 9 that the standard deviations of the $\overline{q_{B/I}}$ are less than 0.05, and for the case using traditional quaternions based kinematics and dynamics the least standard deviation can be converged to less than 0.02. The results verified the analysis

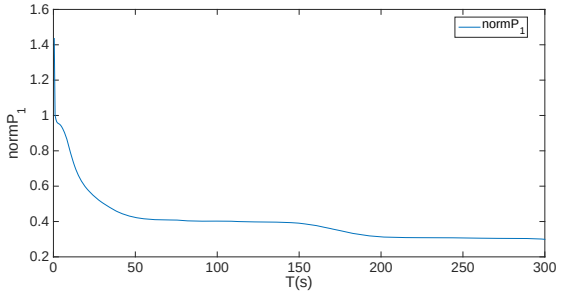

Figure 6: The norm of the state covariance matrix $\|P_1\|$ varying with time

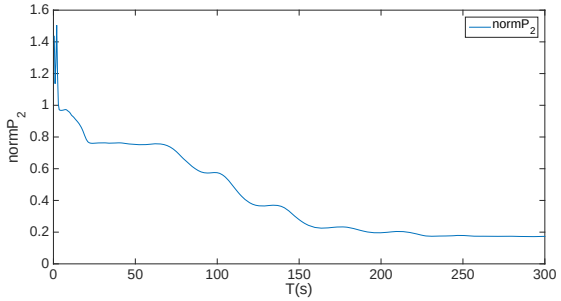

Figure 7: The norm of the state covariance matrix $\|P_2\|$ varying with time

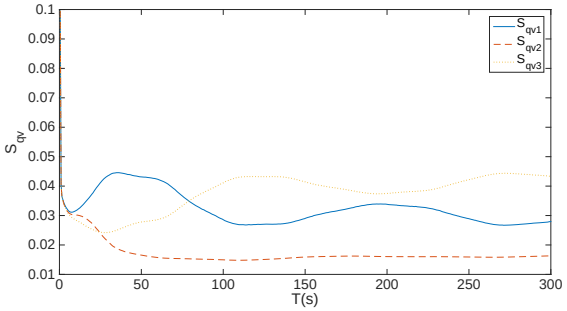

Figure 8: Standard deviations of the $\overline{q_{B/I}}$ by the EKF using traditional quaternions based kinematics and dynamics

in Section 5.4 that the EKF using traditional quaternions based kinematics and dynamics model can provide more accurate estimations of $\overline{q_{B/I}}$. Nevertheless, even if the $\overline{q_{B/I}}$ estimated by the EKF using the DVQ based kinematics and dynamics models has larger errors than the one using the traditional quaternions based kinematics and dynamics, the values can be controlled lower than 0.03, which is acceptable in the parameters estimating missions.

Figs. 10 and 11 illustrate the standard deviations of the ρ by the EKFs using traditional quaternions based kinematics and dynamics and DVQ based kinematics and dynamics

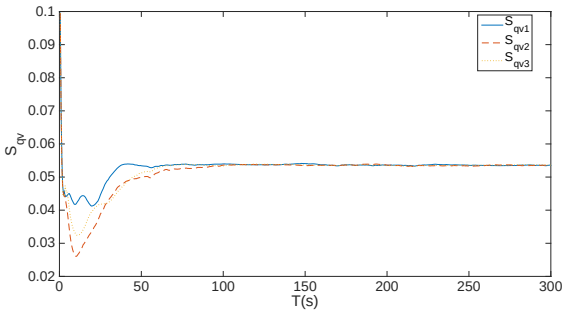

Figure 9: Standard deviations of the $\overline{q_{B/I}}$ by the EKF using DVQ based kinematics and dynamics

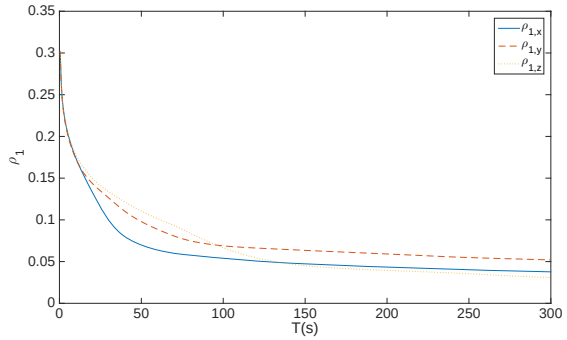

Figure 10: Standard deviations of the ρ_1 by the EKF using traditional quaternions based kinematics and dynamics

respectively. As can be discovered from the simulation results, the standard deviations of ρ_2 are much larger than the ones of ρ_1. This phenomenon happens since the ρ_2 is coupled with the unobservable states v in the DVQ based kinematics and dynamics models. In addition, it can be seen that the time varying tendency of both of ρ_1 and ρ_2 are similar for the reason that ρ_1 and ρ_2 have similar observabilities. However, the accuracies of ρ_1 and ρ_2 are lower than the ones of $\overline{q_{B/I}}$ since the singular values of ρ_1 and ρ_2 are smaller. The results of ρ_1 and ρ_2 also follows the analysis made by Section 5.4.

Figs. 12 and 13 show the standard deviations of the $\omega_{B/I}^{B}$ by the EKFs using traditional quaternions based kinematics and dynamics and DVQ based kinematics and dynamics respectively. It can be discovered that the accuracies of the $\omega_{B/I}^{B}$ from both of the two EKFs are almost the same (lower than 0.05). These results are very good for the estimation of the $\omega_{B/I}^{B}$ since from the analysis in Section 5.4 the $\omega_{B/I}^{B}$ is unobservable and can only be estimated by the EKFs. The estimating results of the $\omega_{B/I}^{B}$ prove that the observability analysis can be utilized as a method to find out which states are observable and have good accuracies. However, the analysis results cannot be utilized to determine the estimating result for a certain unobservable state because the initial errors and estimating algorithm

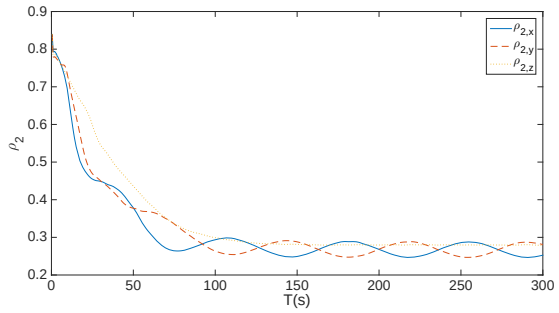

Figure 11: Standard deviations of the ρ_2 by the EKF using DVQ based kinematics and dynamics

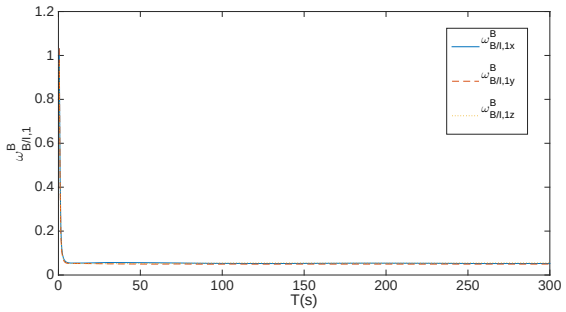

Figure 12: Standard deviations of the $\omega^B_{B/I,1}$ by the EKF using traditional quaternions based kinematics and dynamics

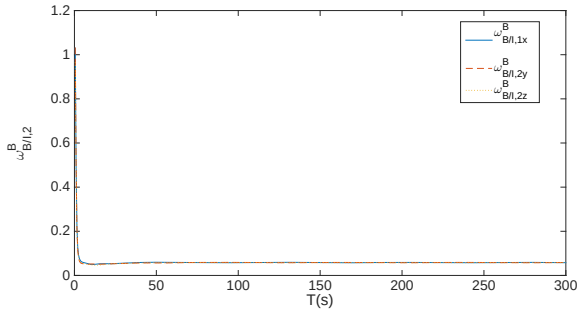

Figure 13: Standard deviations of the $\omega^B_{B/I,2}$by the EKF using DVQ based kinematics and dynamics

are also key ingredients of the parameter estimations.

Figs. 14 and 15 show the standard deviations of the p by the EKFs using traditional quaternions based kinematics and dynamics and DVQ based kinematics and dynamics respectively. As can be seen from the results, since p_1 and p_2 are both unobservable and the initial errors for p are big, the estimating results by the EKFs are not good. the average

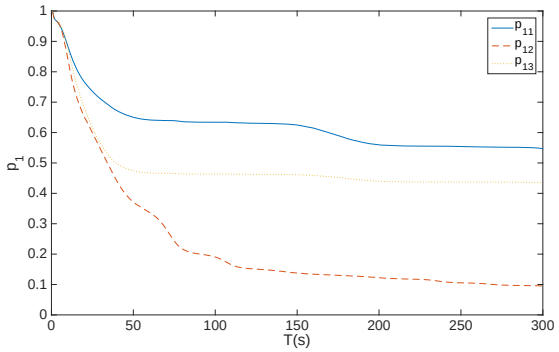

Figure 14: Standard deviations of the p_1 by the EKF using traditional quaternions based kinematics and dynamics

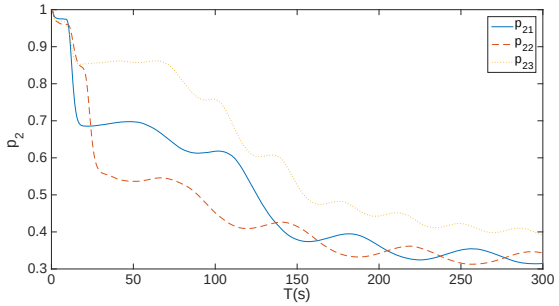

Figure 15: Standard deviations of the p_2 by the EKF using DVQ based kinematics and dynamics

standard deviation is almost 0.4 for p_1 and 0.3 for p_2 . The results revealed that the inertial parameters are sensitive to the initial errors and one must design more robust algorithms to achieve high accuracy estimations.

Figs. 16 and 17 show the standard deviations of the $v^B_{B/I}$ and q_q by the EKF using DVQ based kinematics and dynamics. These two states are about the translational motion which the EKF using traditional quaternions based kinematics and dynamics cannot estimate. In addition, the q_d is the most observable state and $v^B_{B/I}$ is unobservable in the DVQ situation. As can be seen from the results, both of the estimation errors are quite small. The results prove that the former analysis of the observable and unobservable states are reliable. Moreover, the DVQ based kinematics and dynamics model is quite useful in translation parameter estimations due to the simulation results of $v^B_{B/I}$ with large initial errors (0.1 m/s).

5.6 Summary

This section proposes the simulation results of the observability analysis. First of all, the rank of the two OG matrices are calculated. Although the proportions of the observable

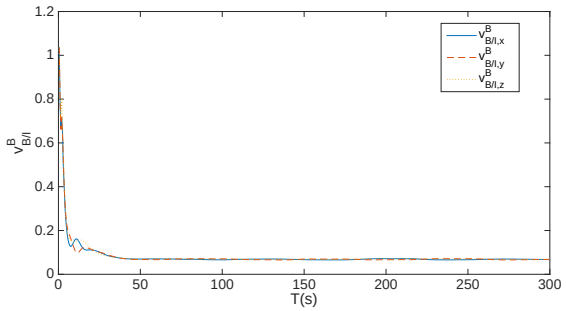

Figure 16: Standard deviations of the $v^B_{B/I}$ by the EKF using DVQ based kinematics and dynamics

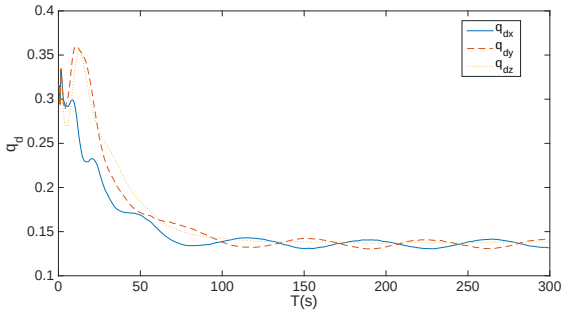

Figure 17: Standard deviations of the q_d by the EKF using DVQ based kinematics and dynamics

parameters are the same, the DVQ based kinematics and dynamics model still has more observable parameters estimated in number. Then, the condition number and SVD analysis are made to reveal the degrees of observabilities of the parameters in both of the two models to show the degree of observability and rank of observabilities of the estimated parameters. Finally, the norm of the covariances of the estimation results and the standard deviations of each of the estimated parameters are given to analyze the observability of each parameter analytically. From the simulation results, if one needs to increase the observabilities of the parameters, more measurements relative to them (i.e., ω, v, p) need to be considered. However, since the sensors for parameter estimations of an uncooperative space target cannot provide contacting information, the proportions of the inertia tensors must be estimated without any relative information. Also, the dynamic parameters (i.e., ω and v) cannot be measured directly since there will not be communications from the uncooperative space target and the dynamic parameters must be calculated from other indirect measurements. under this circumstance, the unobservable parameters (ω, v and p) can only be estimated from the parameters estimating algorithm, which becomes vital important in the parameters estimating missions aiming at the uncooperative space targets. Furthermore, the observability analysis can only tell which state is observable

and find out which observable state has the highest estimating accuracy. Nevertheless, the estimation results of the unobservable states cannot be revealed by the observability analysis. The estimation results of the unobservable states should be discovered by a number of simulations with different initial errors since they are unobservable. Since this paper is focus on the observability analysis of the EKFs using different kinds of kinematic and dynamic models, only one case of initial errors is given. However, the initial errors given by this paper are quite large in the AR&D missions. From the simulation results by Section 5.5, it can be found that EKF using the DVQ based kinematics and dynamics not only has acceptable estimating precision but also outputs "full parameters" estimating results without contacting the uncooperative space target.

6 Conclusion

The observabilities of EKFs with different system models are analyzed by this paper. First of all, the traditional quaternions based kinematics and dynamics model and the DVQ based kinematics and dynamics model (considering translational and rotational coupled effects) are reviewed. Then, the EKFs based on the two different kinds of models are designed. By computing the OG matrices of both of the two models, the observabilities are analyzed numerically and analytically. From the simulation results, the EKF based on traditional quaternions based kinematics and dynamics model can have better observability on the attitude parameters however it cannot estimate the translational parameters in the same time. The EKF based on DVQ based kinematics and dynamics model has lower degree of observability, but it is almost the full-parameters estimation algorithm without contacting the target. Also, the results of covariances varying with time show that the final errors of both of the two designed EKFs are almost the same within the given initial errors, and only some fluctuations occurred in the beginning of the DVQ-EKF estimation procedure. This phenomenon reveals that within the initial errors given by this paper, the DVQ based kinematics and dynamics model can not only provide more information about the parameters but also has a similar accuracy. As a result, the composition of DVQ based kinematics and dynamics model and LIDAR measurements is strongly recommended to be utilized in the parameter estimations missions aiming at uncooperative space targets.

Acknowledgement: The authors wish to express their appreciation to the reviewers for their helpful suggestions which greatly improved the presentation of this paper.

Conflicts of Interest: The authors declare that they have no conflicts of interest to report regarding the present study.

References

Ablin, H. L. (1967): *Criteria for Degree of Observability in A Control System*. Iowa State University of Science and Technology, USA.

Aghili, F. (2012): A prediction and motion-planning scheme for visually guided robotic capturing of free-floating tumbling objects with uncertain dynamics. *IEEE Transactions on Robotics*, vol. 28, no. 3, pp. 634-649.

Aghili, F.; Parsa, K. (2009): Motion and parameter estimation of space objects using laser-vision data. *Journal of Guidance Control & Dynamics*, vol. 32, no. 2, pp. 538-550.

Bageshwar, V. L.; Gebre-Egziabher, D.; Garrard, W. L.; Georgiou, T. T. (2009): A stochastic observability test for discrete-time kalman filters. *Journal of Guidance Control & Dynamics*, vol. 32, no. 4, pp. 1356-1370.

Butcher, E. A.; Wang, J.; Lovell, T. A. (2017): On kalman filtering and observability in nonlinear sequential relative orbit estimation. *Journal of Guidance, Control, and Dynamics*, vol. 40, no. 9, pp. 2167-2182.

Chaves-Jiménez, A.; Guo, J.; Gill, E. (2017): Impact of atmospheric coupling between orbit and attitude in relative dynamics observability. *Journal of Guidance, Control, and Dynamics*, vol. 40, no. 12, pp. 3274-3281.

Crassidis, J.; Markley, F. L. (2003): Unscented filtering for spacecraft attitude estimation. *Journal of Guidance Control & Dynamics*, vol. 26, no. 4, pp. 536-542.

Crassidis, J. L.; Markley, F. L.; Yang, C. (2007): Survey of nonlinear attitude estimation methods. *Journal of Guidance Control & Dynamics*, vol. 30, no. 1, pp. 12-28.

Dai, H.; Jing, X.; Yu, W.; Yue, X.; Yuan, J. (2018): Post-capture vibration suppression of spacecraft via a bio-inspired isolation system. *Mechanical Systems & Signal Processing*, vol. 105, pp. 214-240.

Dong, G.; Zhu, Z. H. (2015): Position-based visual servo control of autonomous robotic manipulators. *Acta Astronautica*, vol. 115, pp. 291-302.

Filipe, N.; Kontitsis, M.; Tsiotras, P. (2015): Extended kalman filter for spacecraft pose estimation using dual quaternions. *American Control Conference*, pp. 3187-3192.

Filipe, N.; Tsiotras, P. (2013): Adaptive position and attitude-tracking controller for satellite proximity operations using dual quaternions. *Journal of Guidance Control & Dynamics*, vol. 38, no. 4, pp. 566-577.

Filipe, N.; Tsiotras, P. (2013): Simultaneous position and attitude control without linear and angular velocity feedback using dual quaternions. *American Control Conference*, pp. 4808-4813.

Flores-Abad, A.; Ou, M.; Pham, K.; Ulrich, S. (2014): A review of space robotics technologies for on-orbit servicing. *Progress in Aerospace Sciences*, vol. 68, no. 8, pp. 1-26.

Friedman, A. M.; Frueh, C. (2018): Determining characteristics of artificial near-earth objects using observability analysis. *Acta Astronautica*, vol. 144, pp. 405-421.

Ham, F. M.; Brown, R. G. (1983): Observability, eigenvalues, and kalman filtering. *IEEE Transactions on Aerospace & Electronic Systems*, vol. AES-19, no. 2, pp. 269-273.

Hou, X.; Ma, C.; Wang, Z.; Yuan, J. (2017): Adaptive pose and inertial parameters estimation of free-floating tumbling space objects using dual vector quaternions. *Advances in Mechanical Engineering*, vol. 9, no. 10, pp. 1-17.

Huxel, P. J. (2009): Navigation algorithms and observability analysis for formation flying missions. *Journal of Guidance Control & Dynamics*, vol. 32, no. 4, pp. 1218-1231.

Jankovic, M.; Paul, J.; Kirchner, F. (2015): Gnc architecture for autonomous robotic capture of a non-cooperative target: preliminary concept design. *Advances in Space Research*, vol. 57, no. 8, pp. 1715-1736.

Kalman, R. E. (1960): A new approach to linear filtering and prediction problems. *Journal of Basic Engineering Transactions*, vol. 82, pp. 35-45.

Krener, A. J.; Ide, K. (2009): Measures of unobservability. *IEEE Conference on Decision & Control*, pp. 6401-6406.

Lefferts, E. J.; Markley, F. L.; Shuster, M. D. (1982): Kalman filtering for spacecraft attitude estimation. *Journal of Guidance Control Dynamics*, vol. 5, no. 5, pp. 417-429.

Liu, C.; Hu, W. (2014): Relative pose estimation for cylinder-shaped spacecrafts using single image. *IEEE Transactions on Aerospace and Electronic Systems*, vol. 50, no. 4, pp. 3036-3056.

Liu, C. S. (2006): The lie-group shooting method for singularly perturbed two-point boundary value problems. *Computer Modeling in Engineering & Sciences*, vol. 15, no. 3, pp. 179-196.

Ma, C.; Dai, H.; Yuan, J. (2017): Estimation of inertial characteristics of tumbling spacecraft using constant state filter. *Advances in Space Research*, vol. 60, no. 3, pp. 513-530.

Opromolla, R.; Fasano, G.; Rufino, G.; Grassi, M. (2017): A review of cooperative and uncooperative spacecraft pose determination techniques for close-proximity operations. *Progress in Aerospace Sciences*, vol. 93, pp. 53-72.

Razgus, B.; Mooij, E.; Choukroun, D. (2017): Relative navigation in asteroid missions using dual quaternion filtering. *Journal of Guidance Control & Dynamics*, vol. 40, no. 1, pp. 1-16.

Segal, S.; Gurfil, P. (2012): Effect of kinematic rotationtranslation coupling on relative spacecraft translational dynamics. *Journal of Guidance Control & Dynamics*, vol. 32, no. 3, pp. 1045-1050.

Wilson, J. A.; Guhe, S. Y. (2005): Observability matrix condition number in design of measurement strategies. *Computer Aided Chemical Engineering*, vol. 20, no. 05, pp. 397-402.

Xing, Y.; Cao, X.; Zhang, S.; Guo, H.; Feng, W. (2010): Relative position and attitude estimation for satellite formation with coupled translational and rotational dynamics. *Acta Astronautica*, vol. 67, no. 3, pp. 455-467.

Yang, C.; Crassidis, J. L. (2004): Particle filtering for sequential spacecraft attitude estimation. *AIAA Paper*, , no. 5337.

Yu, Z.; Cui, P.; Zhu, S. (2014): Observability-based beacon configuration optimization for mars entry navigation. *Journal of Guidance, Control, and Dynamics*, vol. 38, no. 4, pp. 643-650.

Zanetti, R.; DSouza, C. N. (2015): Observability analysis and filter design for the orion earth moon attitude filter. *Journal of Guidance, Control, and Dynamics*, vol. 39, no. 2, pp. 201-213.